Molecular Analysis of Nitrogen Containing Compounds in Vacuum Gas Oils Hydrodenitrogenation by(Esi+/-)-FTICR-MS

Polina Mikhaylova, Luis P. de Oliveira, Isabelle Merdrignac, Alexandra Berlioz-Barbier, Marouan Nemri, Pierre Giusti, Gerhard Pirngruber

Molecular analysis of nitrogen-containing compounds in vacuum gas oils hydrodenitrogenation by (ESI+/-)-FTICR-MS

Polina Mikhaylova[a], Luis P. de Oliveira[a], Isabelle Merdrignac[a], Alexandra Berlioz-Barbier[a], Marouan Nemri[b], Pierre Giusti[b,c], Gerhard D. Pirngruber[a,*]

[a]*IFP Energies nouvelles, Rond-point de l'échangeur de Solaize, BP 3, 69360 Solaize, France*
[b]*TRTG - TotalEnergies Research & Technology Gonfreville, Carrefour n° 4, BP 27, 76700 Harfleur, France*
[c]*International Joint Laboratory−iC2MC: Complex Matrices Molecular Characterization, TRTG Refining and Chemicals, TotalEnergies, 76700 Harfleur, France*

ABSTRACT: This paper is a part of a study on reactivity descriptors in vacuum gas oil hydrotreatment (VGO HDT). It aims to understand the differences in feeds of various process origins and the corresponding hydrotreated effluents on a molecular level. Four different vacuum gas oils were hydrotreated over a sulfided $NiMo/Al_2O_3$ catalyst at a wide range of temperatures and residence times in order to collect HDT effluents at a broad range of hydrodenitrogenation (HDN) conversions. Vacuum gas oils and HDT effluents have been analyzed by Fourier transform ion cyclotron resonance mass spectrometry (FTICR-MS) in positive ESI(+) and negative ESI(-) electrospray ionization modes to characterize the basic and neutral nitrogen-containing species and the subtleties of HDT transformations depending on the feedstock type.

Keywords: vacuum gas oil, hydrotreatment, FTICR-MS

Abbreviations: ESI, electrospray ionization; FTICR-MS, Fourier transform ion cyclotron resonance mass spectrometry; VGO, vacuum gas oil; HDT, hydrotreatment; HDN, hydrodenitrogenation; SR VGO, straight-run vacuum gas oil; HCGO, heavy coker gas oil; HVGO, hydroprocessed vacuum gas oil; GO, gas oil; DMDS, dimethyl disulfide; DBE, double bond equivalent; nC, number of carbon atoms; LHSV, liquid hourly space velocity; AR, atmospheric residue.

*Corresponding author.
E-mail address: gerhard.pirngruber@ifpen.fr (Gerhard Pirngruber)

1. Introduction

Vacuum gas oils represent a valuable source for high-quality refining products. An increase in VGO hydroprocessing is connected with the changes in the composition of currently extracted crude oils and market demand for lighter distillates. VGO consists of a large number of molecules, including heterocyclic ones. Among these heteroatom-containing species, N-compounds are highly problematic. These molecules are poisons for hydrotreating and hydrocracking catalysts, and they exert an inhibitory effect on the removal of other heterocyclic compounds present in VGOs [1–4]. At the same time, nitrogen-containing compounds also inhibit the catalytic cracking conversion of VGO [5,6]. These species must be removed from the VGOs by catalytic hydrotreatment before being subjected to further conversion processes.

In this work, we focus on the HDN reactions, i.e., on the elimination of N-containing species, as these molecules are supposed to be the most refractory for hydrotreatment. In order to explain the refractory behavior of the nitrogen-containing species and the kinetics of VGO HDT, hydrotreatment studies of model molecules as pyridine [7–9], quinoline [10–13], acridine [14], indol [15–17], and carbazole [14] were provided. These studies show the difference in the reactivity and reaction pathways depending on the basic or neutral type of the molecule, the position of the nitrogen atom, and the number of the aromatic rings. Typically, VGO contains derivatives of these model molecules, whose structures are more complex due to additional aromatic or naphthenic rings and/or alkyl side chains [18]. It is important to note that these substituents can significantly influence the molecule's reactivity [19]. In addition, there are several studies dedicated to the identification of HDN refractory species in real feeds as gas oils, vacuum gas oils, and hydrotreated VGO effluents [20–26]. This knowledge is essential for kinetic modelling of the HDT process.

As mentioned earlier, real feeds are affected by the structure of N-compounds and the presence of other molecules. The diversity of structures of N-containing compounds in VGOs is determined by the geochemical origin of crude oil and the process used to obtain VGO [27]. Typical processes for producing VGOs are vacuum distillation of atmospheric residues (straight-run VGO), hydroconversion, fluid catalytic cracking, visbreaking, or coking of heavy residues [28–30]. However, there is still a need to discuss the detailed characterization and a comparison of the transformations occurring in VGOs of different process origins with various conversion degrees in an HDT process. This data is a necessary step in the development of feed-independent kinetic models of VGO hydrotreatment. In this work, we show a unique dataset of VGOs of different origins. Based on it, we have compared the distributions of nitrogen-containing species in HDT effluents from different types of feeds at a wide range of HDN conversion degrees.

FTICR-MS is a high-resolution analytical technique that provides molecular formulas of species containing heteroatoms in a complex hydrocarbon mixture [31]. The application of an electrospray ionization source allows selective analyzing of two types of nitrogen-containing species. The separation of basic and neutral species is important as the molecules within one type have similar reaction pathways, which is essential for reaction network construction [32]. VGOs and HDT effluents have their own "fingerprints," frequently presented in the form of derivatives of Kendrick plots showing the alkylation and aromaticity degrees of the molecules present in the mixture [33,34]. The alkylation degree is determined by the number of carbon atoms (nC). The aromaticity is described by a double bond equivalent (DBE), expressed by Eq.1 for a $C_cH_hN_nO_oS_s$ molecule:

$$DBE = c - \frac{h}{2} + \frac{n}{2} + 1 \quad (1)$$

DBE is a method of calculating the aromaticity or unsaturation degree when the molecular formula is known. It indicates a number of double or triple bonds and rings in the molecule. For

example, DBE=3 may correspond to a structure with 3 rings or 2 rings and one double bond. At the same time, this method gives wrong values for complex organic molecules containing multiple elements, which may have different valence states. The compounds containing halogens have negative DBE values. We use the DBE method as it is a fast and accurate method of determining the aromaticity of the species studied in this work, but we cannot use it to completely distinguish between aromatic structures and hydrogenated structures with additional rings.

The previous studies reported that VGOs contain different heteroatom groups (i.e., *N1*, *NxSy*, *S1*, *OxNy*), but the *N1* class (only one nitrogen atom in the structure) is predominant. In addition, multi-heteroatom species are very quickly removed during hydrotreatment or reduced to a very small residual concentration [33]. In this work, we focus on the comparison of the species and their families containing only one nitrogen atom in a structure.

This paper begins with a description of the pilot tests and experimental conditions used for obtaining HDT effluents, physicochemical characteristics of the studied VGOs and corresponding effluents. We present the conditions applied for the (ESI+/-)-FTICR-MS analysis. The next section contains the results of the comparison of the effluents at different HDN conversion degrees by DBE and the number of carbon atoms. In the discussion section, we propose mechanisms for VGO HDN based on the obtained data and compare our results with the relevant studies of heavier and lighter cuts. Our conclusions and perspectives of the study are drawn in the final section.

2. Experiments and methods

2.1. Feedstocks

The feedstocks are four industrial vacuum gas oils of different types: two straight-run vacuum gas oils (SR VGO) obtained from direct distillation of crude oils, one heavy coker gas oil (HCGO)

89 produced via a thermal conversion process, and one hydroconverted vacuum gas oil (HVGO)
90 obtained via hydroprocessing of heavy residues.

91 *2.2. Pilot tests*

92 The VGO hydrotreatment tests were performed in a pilot unit equipped with an up-flow fixed-
93 bed catalytic reactor over a $NiMo/Al_2O_3$ commercial catalyst. The experimental unit can be divided
94 into three major sections: the feed, the reaction, and the separation section (Fig. A.1). The feed
95 section consists of the hydrogen line (purity=99.5 %) and the hydrocarbon liquid feed section. The
96 hydrocarbon feed section is composed of two feed tanks (in Fig. A.1, only one tank is illustrated)
97 and two transfer pumps. To keep the feed in a liquid phase, these pieces of equipment are inside
98 the heated enclosure. The hydrocarbon feed and H_2 are injected together from the bottom of the
99 reactor via a mixing gas-liquid inlet. The reactor itself is a steel tube with a volume of 165 cm^3
100 and with an internal diameter of 19 mm. The catalytic bed is packed with glass balls (0.5 mm
101 diameter) and carborundum layers. A 1 cm grid is placed at the end of the catalytic bed in order to
102 hold the catalyst in place. The catalyst's volume is 50 cm^3 with an additional 10 cm^3 of catalyst
103 guard bed, protecting the main catalyst from deactivation by metals.

104 Four heating shells around the reactor provide an isothermal axial temperature profile in the
105 catalyst zone. Each heating shell contains an external thermocouple. The internal thermal profile
106 is controlled and regulated by four internal thermocouples (TC). These four TCs are spread over
107 the height of the reactor in order to have an internal measurement per heating shell.

108 Before entering the separation section, the reactor effluent is kept at a high temperature to
109 prevent plugging caused by the creation of ammonium sulphide crystals. The high-pressure
110 separator V1 separates the effluent into a liquid phase, which will be sent to the collecting tank,

and a gas phase, which will be directed to the separator V2. Separated gases from V2 are sent automatically to gas chromatography every 4 hours.

Operating conditions were chosen by preliminary simulation of HDT and HDN performance to cover the full range of conversion of nitrogen-containing species in the pilot tests. All pilot tests were started from a reference point with the same VGO feed to check the repeatability of the experiments. The reference point was repeated to evaluate the catalyst deactivation at the end of each test. To control the stabilization of the experimental points, we monitored the macroscopic properties (density, refractive index, sulphur, and total nitrogen content) of the liquid phase and the composition of gas effluents. Once we achieved stable operation, a mass balance was performed, taking into account analyses of the feed (gas + VGO) and the product (online gas analysis + hydrotreated effluent).

Pilot tests were carried out under the conditions described in Table 1 for a period of 38-45 days. The conversion of the nitrogen in the effluent after hydrotreatment was calculated via the following equation (Eq.2), where $c[N]_i$ - the content of the total nitrogen in the VGO (in ppm) and $c[N]_o$ - the content of the total nitrogen in the hydrotreated effluent (in ppm):

Table 1

Pilot tests operating conditions.

H_2 partial pressure, bars	120
Temperature, °C	T_{ref}-20 - T_{ref}+35
LHSV, h^{-1}	$LHSV_{ref}$-0.9 - $LHSV_{ref}$+2.1
H_2/HC ratio, NL/L	900

$$HDN = \frac{c[N]_i - c[N]_o}{c[N]_i} \cdot 100\ \%\ (2)$$

2.3. (ESI+/-)-FTICR-MS

VGOs and effluents were analyzed by FTICR-MS in ESI(+) and ESI(-) modes to characterize basic and neutral nitrogen compounds, respectively. In order to assess the reproducibility of the tests, three replicate analyses were carried out on each sample. Mass spectrometry was done using an LTQ FT Ultra Mass Spectrometer FTICR-MS (ThermoFisher Scientific) equipped with a 7T magnet (Oxford Instruments), with an ESI source (ThermoFisher Scientific, Bremen, Germany). The data acquisition range was set to m/z of 98-1000, with 200,000 initial resolution, and 70 scans were collected for each sample. The transient signal was recorded to enable further data processing. The ionization parameters were used based on the results of Guillemant's FTICR-MS study of nitrogen compounds in gas oils [35].

The samples with a total nitrogen content above 100 ppm were prepared using a VGO concentration of 0.5 mg/mL in a toluene-methanol solvent in a proportion of 75:25 % v/v with 1% of additive (acetic acid or ammonium hydroxide depending on the ionization mode). For samples with a total nitrogen content of less than 100 ppm, the (ESI+)-FTICR-MS data was too noisy under these conditions. In order to avoid this problem, these samples were prepared using a higher VGO concentration of 1 mg/mL. Fig. A.2 presents the comparison of the basic family distributions by relative intensities for effluent B3 (Table A.1), originating from SR VGO B, and obtained at 88 % of HDN, containing 339 ppm of nitrogen. This nitrogen content allows obtaining (ESI+)-FTICR mass spectra for the samples prepared with low and higher concentrations of VGO. The results show good reproducibility of the peak intensities at elevated concentrations, enabling comparison of all hydrotreated effluents samples.

PeakByPeak and Autophaser commercial software provided transient summation, phase correction, threshold noise extraction, peak selection, and mass recalibration. More details on the used processing procedure can be found in the work of Guillemant et al. [36].

Obtaining a quantitative composition by (ESI)-FTICR-MS remains an unachievable task due to the non-uniform ionization of the molecules. For the semi-quantitative characterization of the N-containing species, we used the approach described in the Nguyen et al. study [20]. Pseudo-concentrations are presented as the product of the relative intensities in ESI(+) or ESI(-)-FTICR-MS spectra and the basic/neutral nitrogen content of the VGO or its HDT effluents.

As previously stated, in this study, we focused on the families of the *N1*-class. To characterize the species of this class, we linked the corresponding DBEs to each family, named after the simplest structure (without side alkyl chains and extra aromatic or naphthenic rings) representing the family. Fig. 1 describes the representative structures and DBE intervals for the studied *N1* families.

3. Characterization of feedstocks and effluents

In this work, feeds and liquid effluents were analyzed by standard petroleum analyses and (ESI+/-)-FTICR-MS. Table A.2 describes the standards or the methods of the used analyses.

The physicochemical properties obtained from standard petroleum analyses of the feeds and corresponding liquid effluents are given in Table 2 and Table A.1. More details on the simulated distillation curves of the studied vacuum gas oils can be found in Fig. A.3. Besides the process origin, the selected feeds differ by the content of total nitrogen, basic nitrogen, sulfur, and density. Feeds C and D, which originate from conversion processes of heavier fractions, have higher nitrogen contents than the SR VGOs A and B. Feed D has a particularly low sulfur content since

it is a product of hydrotreating. The initial and final boiling points of the feeds vary from 227 to 291 °C and 588 to 603 °C, respectively. Feed C is the lightest one of the four VGOs.

More details on the differences between the feeds can be observed by comparing the DBE vs. the number of carbon atom plots in Fig. 2. Additional information can be extracted from these plots using a planar limits approach, which allows evaluating the difference in the types of the present structures in vacuum gas oils [26,37]. In the DBE-nC plots, we estimate the slope of the line that connects the points with the highest DBE at the range of numbers of carbon atoms in the N-containing species. In Fig. A.4, three variants of planar limits slopes are demonstrated by the example of the basic nitrogen-containing molecules. The slope of 0.75 implies an increase in DBE by 0.75 per carbon atom, which corresponds to the linear addition of an aromatic ring. If a slope is above 0.75 (DBE is increased by more than 0.75 per carbon atom), it indicates a non-linear aromatic ring addition. The slope below 0.75 is characteristic of a saturated ring or an alkyl chain addition. The same interpretation of the slopes is also applicable to the neutral type of nitrogen-containing species.

3.1.Characterization of straight-run VGO A

SR VGO A has the lowest total nitrogen content and the lowest density (Table 2) among the four feeds. The boiling range of this feed is 285-602 °C, and the nitrogen to sulphur ratio (N/S) is 0.09.

For the SR VGO A (left column in Fig. 2), the basic *N1* molecules are characterized by a DBE range of 4-22 and carbon numbers 11-61 with highly intensive peaks (relative intensity above 40 %) at DBE 7-13 and carbon numbers 25-44. The carbon number distribution for basic nitrogen species in VGO A is centered between 30 and 35 carbon atoms, with the maximum at DBE=9 (quinoline with two saturated rings structures). In the case of SR VGO A, the planar limit slope is close to 0.75. It means that for basic N-species of SR VGO A with an increase in DBE from 8 to

18, the structures of the species represent the product of the linear addition of aromatic rings to structures with a lower DBE.

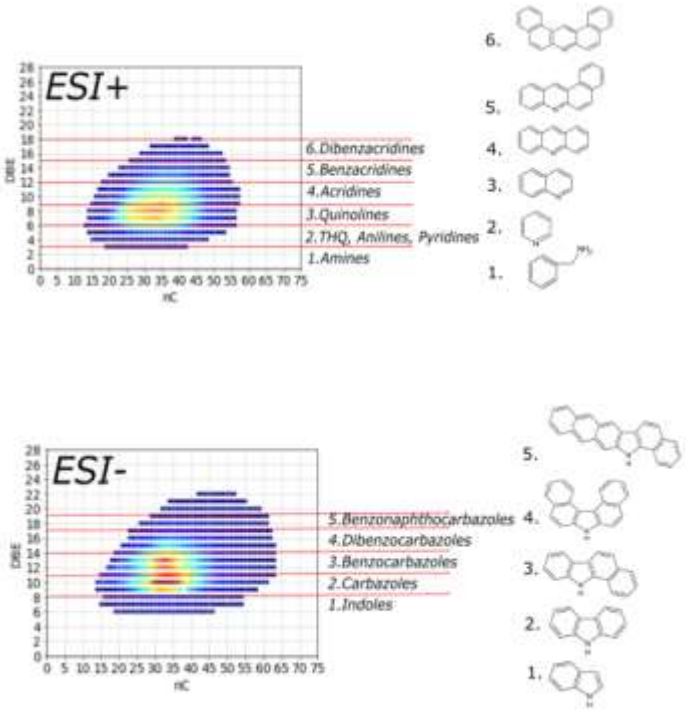

Fig. 1. *N1*-families representative structures and corresponding DBE ranges for ESI+ and ESI- modes.

When comparing the DBE vs. a number of carbon atom plots for neutral *N1* species (right column in Fig. 2) in VGO A, one can see that the distribution is characterized by the range of DBE=6-22 and the range of carbon atoms nC=15-57. The most abundant peaks are found at DBE=12 and DBE=13 (benzocarbazoles) in the range of nC from 30 to 35. VGO's A DBE-nC plot obtained in negative ESI mode shows a slope characteristic for linear aromatic addition.

3.2.Characterization of straight-run VGO B

SR VGO B has a medium total nitrogen content and the highest density (Table 2) among the four feeds. The boiling range of this feed and N/S ratio are very close to SR VGO A and equal to 291-603 °C and 0.08, respectively.

For the SR VGO B, the basic *N1* molecules distribution is characterized by a DBE range of 4-19 and carbon numbers 11-58 (Fig. 2). The most intensive peaks (relative intensity above 40 %) are located at DBE=7-13 and carbon numbers 25-44, similarly to SR VGO A. The carbon number distribution for basic nitrogen species in VGO B is centered between 30 and 35 carbon atoms, with the maximums at DBE=8 and DBE=9 (quinoline structures with one and two saturated rings, respectively). The planar limit slope is 0.76, i.e., the same as in SR VGO A.

The differences at the molecular level between two straight-run VGOs are more evident when comparing the DBE vs. a number of carbon atom plots for neutral N-species. SR VGO B has a narrower DBE-nC distribution (DBE=9-20, nC=16-50) compared to VGO A. The common feature in the two SR VGOs is the location of the most abundant peaks at DBE=12 and 13 and the most intensive species have from 30 to 35 carbon atoms. In contrast to the basic nitrogen distributions, the two SR VGOs have different slopes of planar limits of the neutral N-species (Fig. 2). The slope of VGO B is lower than 0.75, indicating the addition of saturated carbon atoms with an increase in DBE.

3.1.Characterization of heavy coker gas oil VGO C

HCGO VGO C has a high total nitrogen content and a medium density (Table 2). The initial boiling point of this feed is low (227 °C), and the final boiling point is lower than in the SR VGOs (588 °C). VGO C's N/S ratio is twice higher than in SR VGOs.

The basic *N1* species in VGO C are located in the zone DBE 4-27 and carbon numbers 10-56. In comparison to SR VGOs, the most abundant peaks in HCGO are in the similar zone of DBE 7-13, but these species have shorter alkyl side chains (nC 21-33). The most abundant species in HCGO are quinolines with two saturated rings (DBE=9) and acridines (DBE=10). For VGO C, a slope below 0.75 was observed, which can probably be explained by the presence of saturated

rings addition. One can see that for HCGO VGO C, the most abundant peaks are close to the planar limit, which is related to the short alkyl chains of nitrogen compounds in this type of feed.

The most abundant neutral nitrogen species in HCGO are presented only by a few separate points with an alkylation degree of less than 26 carbon atoms at DBE=12, 15, and 18. For neutral N-species, the slope of the planar limit was also below 0.75.

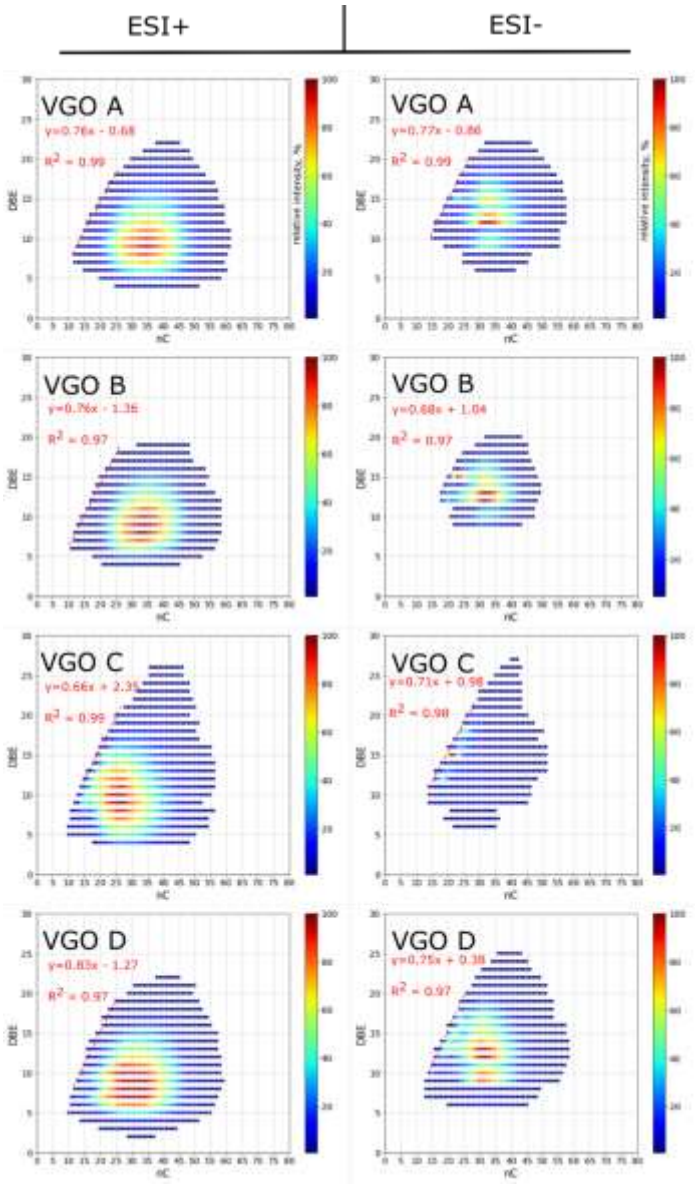

Fig. 2. DBE vs. carbon atom number plots for basic (ESI+ column) and neutral (ESI- column) *N1* compounds in the feeds (VGO A, VGO B - SR VGO, VGO C - HCGO, VGO D - HVGO).

Table 2

Physicochemical properties of the feeds.

Sample	d_{15}, g/cm3	N total, wppm	N basic, wppm	N neutral, wppm	S, wppm	IBP, °C	FBP, °C
VGO A (SR VGO)	0.9212	1440	396	1044	15620	285	602
VGO B (SR VGO)	0.9787	2650	697	1953	34600	291	603
VGO C (HCGO)	0.9495	3425	892	2533	16720	227	588
VGO D (HVGO)	0.9317	3640	1059	2581	3409	264	589

3.2.Characterization of hydroconverted vacuum gas oil VGO D

HVGO VGO D has the highest total nitrogen content and medium density (Table 2). The initial boiling point of this feed is 264 °C and the final boiling point is the same as that of VGO C, 589 °C. VGO D has the highest N/S ratio of the four feeds.

Regarding *N1* basic species in HVGO (VGO D), one can see that its fingerprint is located in the DBE zone with values 2-22 and nC values 10-59. The most intensive peaks are slightly less aromatic (DBE range 6-11), and their alkylation degree is wider compared to the three other feeds. The most abundant basic nitrogen species in HVGO have 25-35 carbon atoms. The slope of the planar limit is 0.83, which indicates the presence of peri-condensed aromatic rings.

The distribution of neutral N-species in VGO D looks similar to SR VGO A. However, the most abundant species are more intensive at DBE=9-10 and 12-13, which are centered at 30-35 carbon atoms. The planar limit slope of VGO D is also close to the value of the slope in VGO A, which shows a linear addition of aromatic cycles.

The essential advantage of the selected feeds is the difference in the DBE-nC distributions of the abundant neutral and basic species, which makes it possible to work with a wide variety of structures. It is important to note that the distributions of the most intensive peaks share common

trends for VGOs of the same type (i.e., SR). For better understanding, the simplest hypothetical structures of the most abundant species in each feed are illustrated in Fig. A.5.

4. Results

In order to evaluate the reactivity of the feeds, the HDN conversion as a function of temperature was compared for each feed. Fig. 3 shows the dependence of HDN on the temperature in the reactor at a constant liquid hour space velocity (LHSV). According to the plot, SR VGO A demonstrated the highest reactivity, closely followed by HCGO (VGO C) and SR VGO B. HVGO (VGO D) showed the lowest reactivity during the pilot tests.

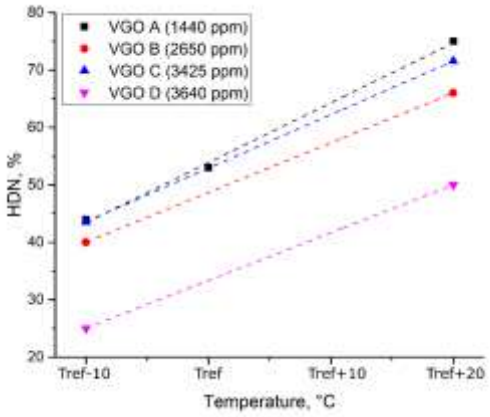

Fig. 3. Comparison of the feeds reactivity (experimental HDN vs. temperature in the reactor) at fixed LHSV.

To better understand the differences between the selected feeds during HDT, we have provided a comparison of the distributions of neutral and basic families as a function of HDN conversion. It is worth noting here that during hydrodenitrogenation of all feeds we observed a slight increase in the basic nitrogen compounds' fraction at the beginning of the hydrotreatment (Fig. 4). It can be explained by the fast consumption of the neutral nitrogen species or by the transformation of

neutral nitrogen species into basic ones. At high HDN conversions, however, the basic nitrogen species were almost completely converted, and the majority of the "refractory" (or residual) nitrogen species were neutral ones, which is explained by reactivity differences due to competitive adsorption on the catalyst's surface [14,17,38]. While all feeds follow the same global trend, the operating conditions also impact the basic fraction. This is visible for VGO A, where we observed two very different values for the basic nitrogen fraction at close to 75 % HDN conversion. This is attributed to different reaction temperatures: at a given conversion, a lower temperature led to a higher fraction of basic nitrogen in the effluent. More peculiarities of these effects in vacuum gas oils can be provided after a detailed analysis of the nitrogen families' transformations as a function of HDN degree.

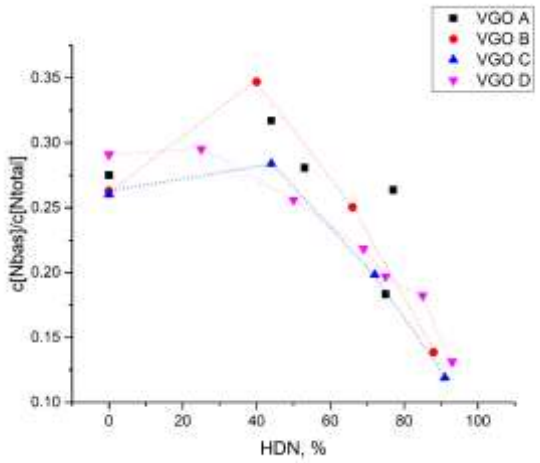

Fig. 4. Change in the proportion of basic nitrogen as a function of HDN level.

4.1. Transformation of basic and neutral nitrogen species

4.1.1. Changes in DBE distributions for SR VGO A

A comparison of the distributions of the basic nitrogen families as a function of DBE is shown in Fig. 5. A normal distribution was observed for SR VGO A and its effluents at all conversion degrees. The distribution maximum shifted from DBE=9 to DBE=7 at the start of hydrotreatment,

and the pseudo-concentration of the families with DBE=7-20 decreased. The DBE shift of -2 happened due to the hydrogenation of one aromatic ring in the highly aromatic structures. After 53 % of HDN, the structures with DBE=8 were the most abundant in the effluents. The distribution of families in the hydrotreated effluents ranged from amines (DBE=2) to dibenzacridine families (DBE=18). The full transformation of the most aromatic basic species (DBE=16 and higher) was observed only at 96 % of HDN.

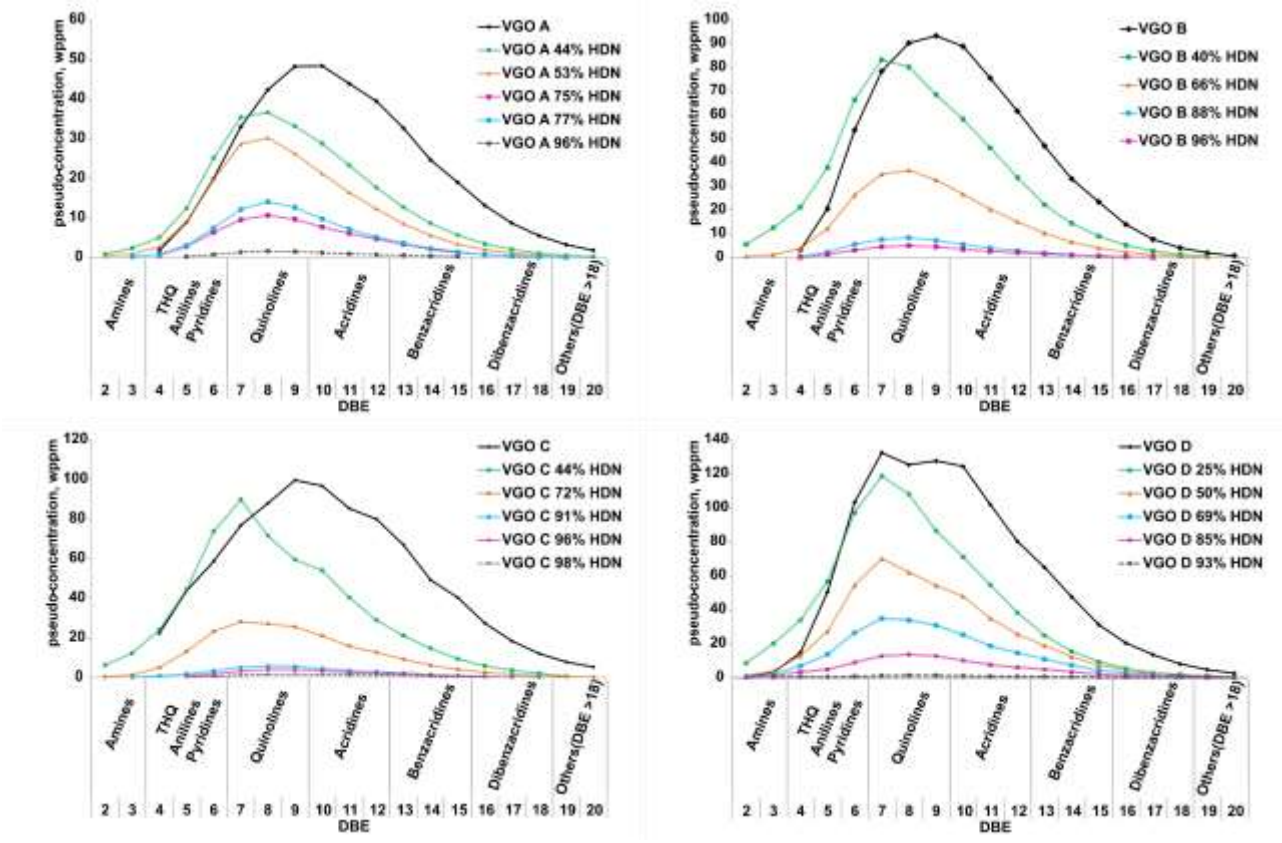

Fig. 5. The distributions of the basic nitrogen families at different HDN conversion degrees.

Fig. 6 reports a detailed comparison of neutral nitrogen families. As one can see, SR VGO A has a trimodal distribution for the initial feed (the carbazole, benzo- and dibenzocarbazole families had the most intensive peaks) with a high proportion of benzocarbazoles with DBE=12.

The trends for the neutral nitrogen species show rapid consumption of the neutral species with high DBEs as benzocarbazoles, dibenzocarbazoles, and benzonaphtocarbazoles at early hydrotreatment stages. After 44 % of HDN, a slow uniform consumption of the carbazoles and benzocarbazoles was observed. Even at high conversion degrees, some amounts of the species at DBE range from 9 to 15 remained in the effluents.

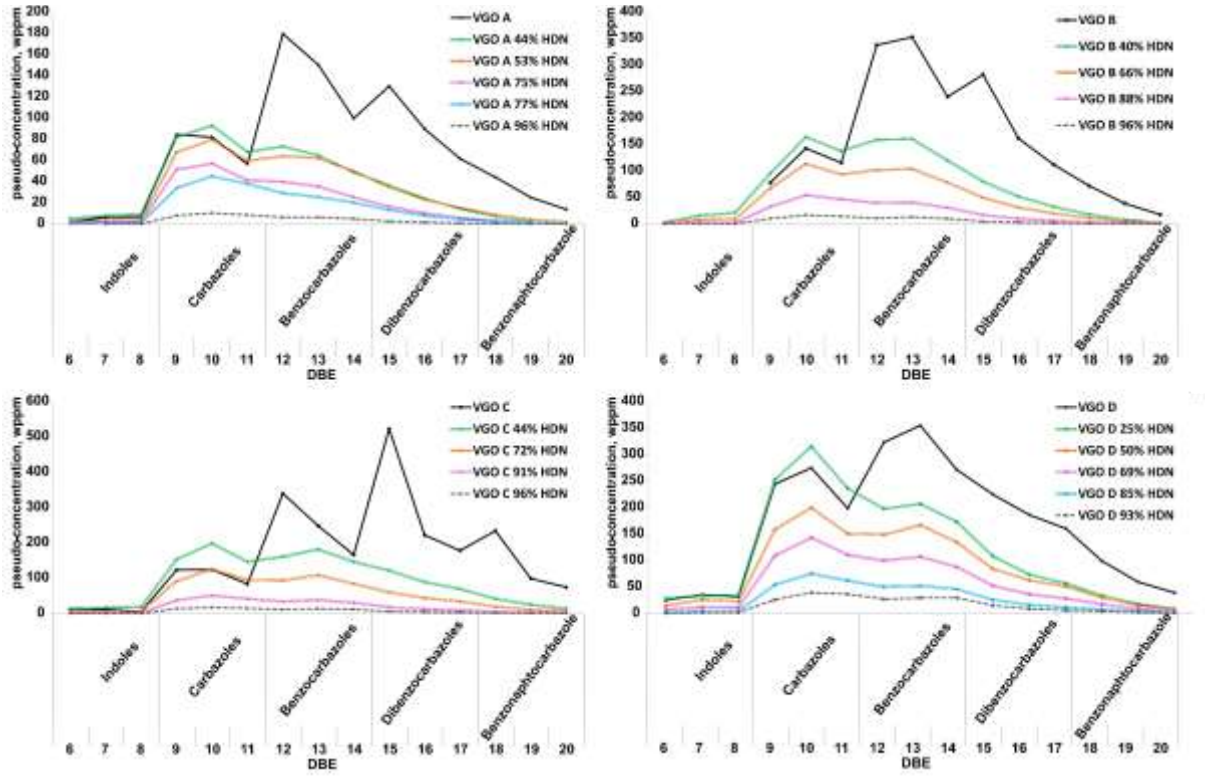

Fig. 6. The distributions of the neutral nitrogen families at different HDN conversion degrees.

4.1.2. Changes in DBE distributions for SR VGO B

The second SR VGO B and its effluents also demonstrate a normal DBE distribution for basic N-species (Fig. 5), spanning from amines to dibenzacridines at conversion degrees up to 88 % of HDN. As for SR VGO A, we observed a shift of the distribution maximum from DBE=9 to DBE=7 in the early process. Species with DBE=7 predominated at a low conversion rate (HDN=40%) in VGO B. At higher HDN conversion, the maximum shifted to DBE=8.

Concerning neutral N-species in SR VGO B, similar to SR VGO A, a trimodal distribution was observed for the initial feed, with a predominance of benzocarbazoles with DBE=12 and DBE=13 (Fig. 6). Analogous to the first SR VGO, the neutral species with DBE above 12 were rapidly consumed at the beginning of hydrotreatment. After 44 % of HDN, there was a slow uniform consumption of the carbazoles and benzocarbazoles.

4.1.3. Changes in DBE distributions for HCGO VGO C

In the case of basic nitrogen-containing species in HCGO VGO C, the distribution's maximum shifted from DBE=9 to DBE=7 at the beginning of the hydrotreatment and after then returned to DBE=9 with increasing HDN (Fig. 5). This behavior could be attributed to the fast hydrogenation of species with DBE=9, leading to the increase of species with DBE=7 at the beginning of HDT and to the sluggish hydrogenation of DBE=10-13 species whose pseudo-concentration is quite high in the HCGO, leading to the shift back to DBE=9 at higher conversion.

HCGO has a DBE distribution for neutral species with four peaks at carbazole, benzo- and dibenzocarbazole and benzonaphtocarbazole families. In the first HDT effluent (44 % of HDN), one can see a very quick consumption of a part of benzocarbazoles, dibenzocarbazoles, and species with DBE=18 (Fig. 6).

4.1.4. Changes in DBE distributions for HVGO VGO D

We observed a different DBE distribution pattern for the basic N-species in the hydroconverted VGO D compared to the previous three feeds. The first thing that is striking is the wider DBE distribution, which is typical for HVGO, which is the product of hydrotreatment of heavier feeds (Fig. 5). Likewise, the shift from DBE 9 to 7(8) was not observed, presumably because the feed had already been hydrotreated, which means that the shift had already occurred in the feed.

The effect of preliminary feed hydrotreatment is also visible in the neutral species, where the fraction of species with DBE=10 and DBE=12 is significantly higher than in other feeds (Fig. 6).

4.2. Changes in alkylation degree

In order to verify the origin of basic nitrogen species (hydrogenation of the basic species with higher DBE vs. hydrogenation of the neutral species) and to understand the HDN reaction mechanism of the species, it will be informative to study the carbon number distributions for the most abundant DBEs for basic and neutral species and for those with higher DBEs that are likely to be the source of abundant species in the HDT effluents. Fig. 7-8 show the carbon number distributions for all N-families and conversion degrees for positive and negative electrospray ionization modes, respectively. Substantial information about species' reactivity can be extracted by a detailed analysis of these distributions for all N-families.

4.2.1. Changes in carbon number distributions for SR VGO A

For VGO A, the less alkylated basic nitrogen species were rapidly consumed at the beginning of hydrotreatment (Fig. 7), leading to a shift of the distribution's maximum to the right. The least reactive basic species had a carbon number above 47. For the neutral species, all carbon numbers diminished to roughly the same extent at the early stages; the distribution shifted to heavier species only at higher conversion levels (Fig. 8).

To extract more information about the origin of the most abundant species in the effluents, the carbon number distributions for basic species in VGO A with DBE=7, DBE=8, DBE=9, DBE=11 were compared (Fig. A.6). From the study of DBE distributions described in the previous section, it was found that there was a shift towards quinolines and species with DBE=7 at the beginning of hydrotreatment. Comparing the carbon number distributions for these species, one can see consumption of the quinolines with DBE=7 and carbon atoms from 24 to 36, while heavier ones

were slightly accumulated. The accumulation of DBE=7 species compared to initial feed can be related to the hydrogenation of quinolines with DBE=9, resulting in structures with one aromatic cycle. At the same time, quinolines and species with DBE=9 can originate from acridines with one saturated cycle characterized by DBE=11. Quinolines with DBE=9 and carbon atoms in the range 14-45 were rapidly consumed, whereas the pseudo-concentration of species with a number of carbon atoms above 45 remained at the same level as in the initial feed. The accumulated DBE=7 species with higher carbon atom numbers (in the case of VGO A, above 45) were probably generated from neutral nitrogen species.

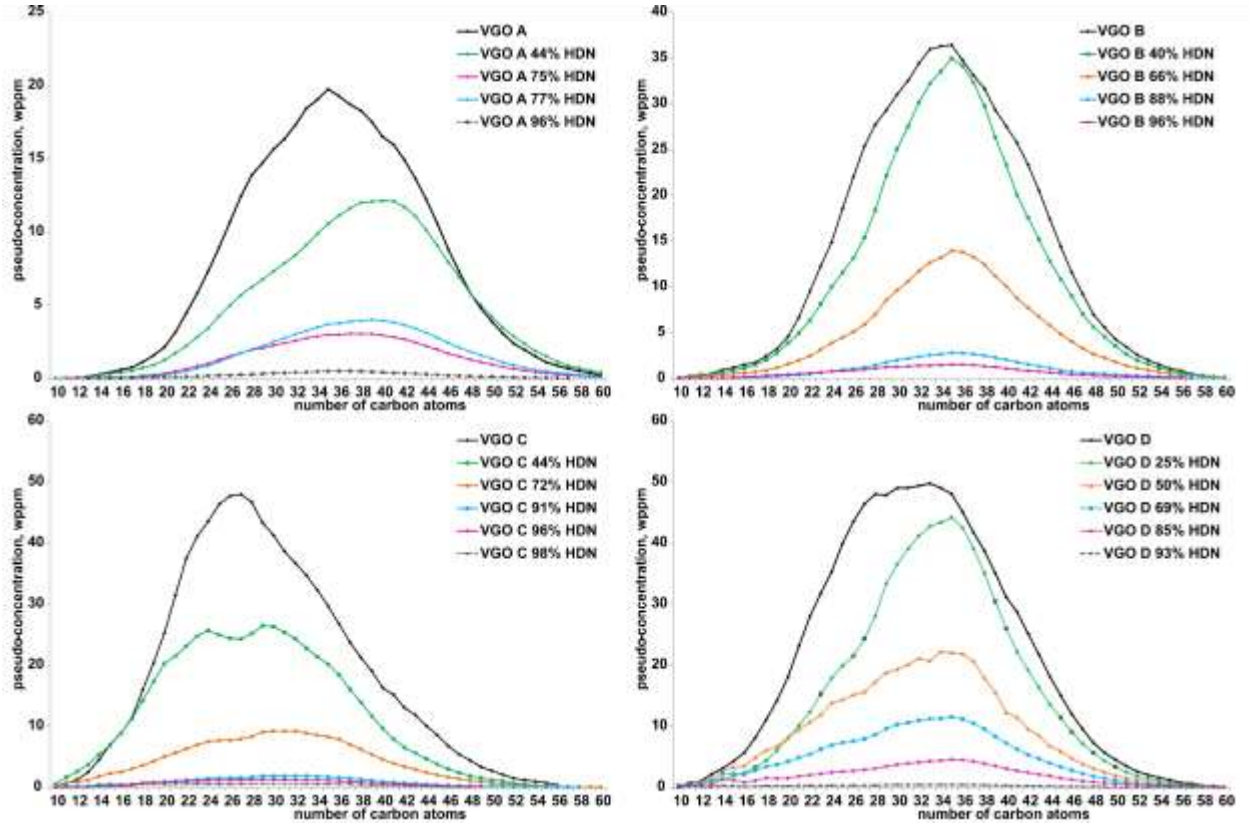

Fig. 7. The carbon number distributions of the basic nitrogen families at different HDN conversion degrees.

377 The shift of the carbon distributions' maximum from 35 to higher carbon numbers at the
378 beginning of the hydrotreatment indicates a higher reactivity of species with low carbon number
379 in the feed.

380 In Fig. A.7, the carbon number distributions are shown for the most abundant neutral nitrogen-
381 containing families in DBE distributions: carbazoles with DBE=10, benzocarbazoles with
382 DBE=12 and their potential sources - families with DBE=14 and DBE=16. Carbazoles with
383 DBE=10 may originate from benzocarbazoles with DBE=12 by hydrogenation of an external
384 aromatic cycle. At the early stages of HDN, the consumption of carbazoles and their generation
385 by hydrogenation of benzocarbazoles are in balance.

386

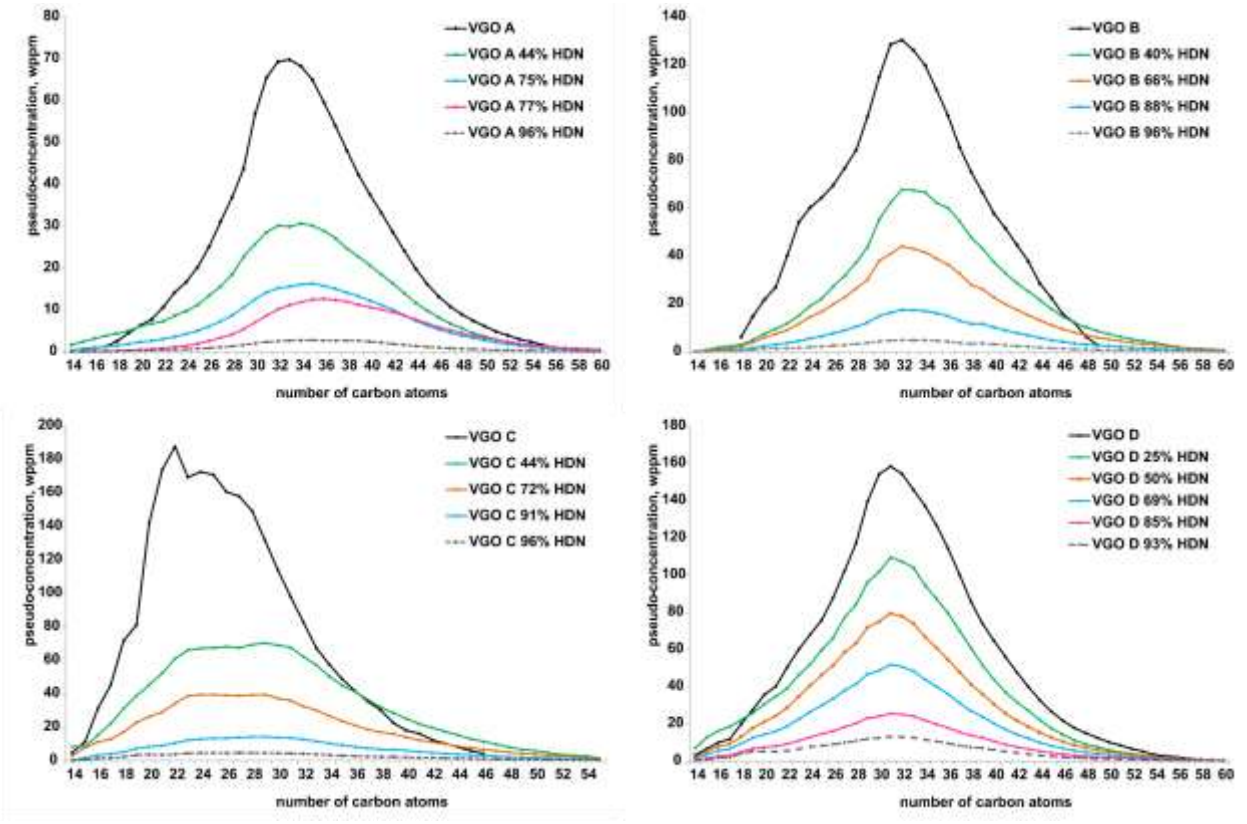

387

388 **Fig. 8.** The carbon number distributions of the neutral nitrogen families at different HDN
389 conversion degrees.

390 *4.2.2. Changes in carbon number distributions for SR VGO B*

391 For VGO B, basic nitrogen species hardly diminished at low HDN level, probably due to a
392 transfer from the neutral to the basic fraction; in contrast to VGO A, there was no change in the
393 distribution of carbon numbers (Fig. 7). As for the neutral species, they diminished more quickly
394 at low conversion, without any marked change in the carbon number distribution (Fig. 8). In the
395 distribution of carbon numbers for neutral nitrogen species, one can see the generation of highly
396 alkylated species within the HDN level. We attribute this to the semi-quantitative nature of the
397 analytical technique or to the possible generation of these neutral N-species from the other
398 heteroatom-containing minor classes as *N1Ox*, *N1Sx*, etc., during the hydrotreatment.

399 As in the previous VGO, the carbon number distributions for the most abundant basic and neutral
400 N-species in VGO B were compared (Fig. A.8-A.9), and trends qualitatively similar to those in
401 the case of SR VGO A were observed.

402 *4.2.3. Changes in carbon number distributions for HCGO VGO C*

403 We noted a faster consumption of highly alkylated basic species in the carbon number
404 distribution for VGO C (Fig. 7), i.e. the opposite trend than in feed A. As for the carbon number
405 distribution for neutral nitrogen species shown in Fig. 8, effluents were found to have a broader
406 distribution compared to the initial feed. The generation of highly alkylated neutral compounds
407 within HDN conversion is also assumed to be an artefact, attributed to the conversion of *N1Ox*
408 and/or *N1Sx* species to the *N1* family.

409 As can be seen from Fig. 9, for species with DBE=7, there was a strong accumulation of basic
410 species with 14 and 20 carbon atoms at the early HDT stages. Comparing these results with the nC
411 distribution for neutral species (Fig. 10), we observed a very fast consumption of a peak of
412 DBE=12 species (benzocarbazoles) with a low carbon number. We assume that full hydrogenation

of the aromatic cycle next to the heteroatom-containing ring occurred, leading to its transition into basic-type species with DBE=7. The light species with C14 probably also originated from neutral nitrogen species, containing five-membered cycles. Hypothetical structures with DBE=7 and 14 carbon atoms are suggested in Fig. 9. Given that the basic species with DBE=9 and DBE=11 are consumed uniformly throughout the nC range, they also can contribute to the accumulation of the species with DBE=7, but do not explain the peak at 20 carbon atoms. For DBE=9 and DBE=11, a bimodal distribution was observed. We evoke the hypothesis that the bimodal distribution arises from the simultaneous presence of structures with different numbers of rings, i.e. in the case of DBE=9, three-rings (acridine), and four-rings (dinaphtoquinoline) and the presence of the peri-condensed structures. The hydrogenation of DBE=9 compounds responsible for the peak at low carbon numbers could explain the peak at C14 in the DBE=7 distribution at low HDN conversion.

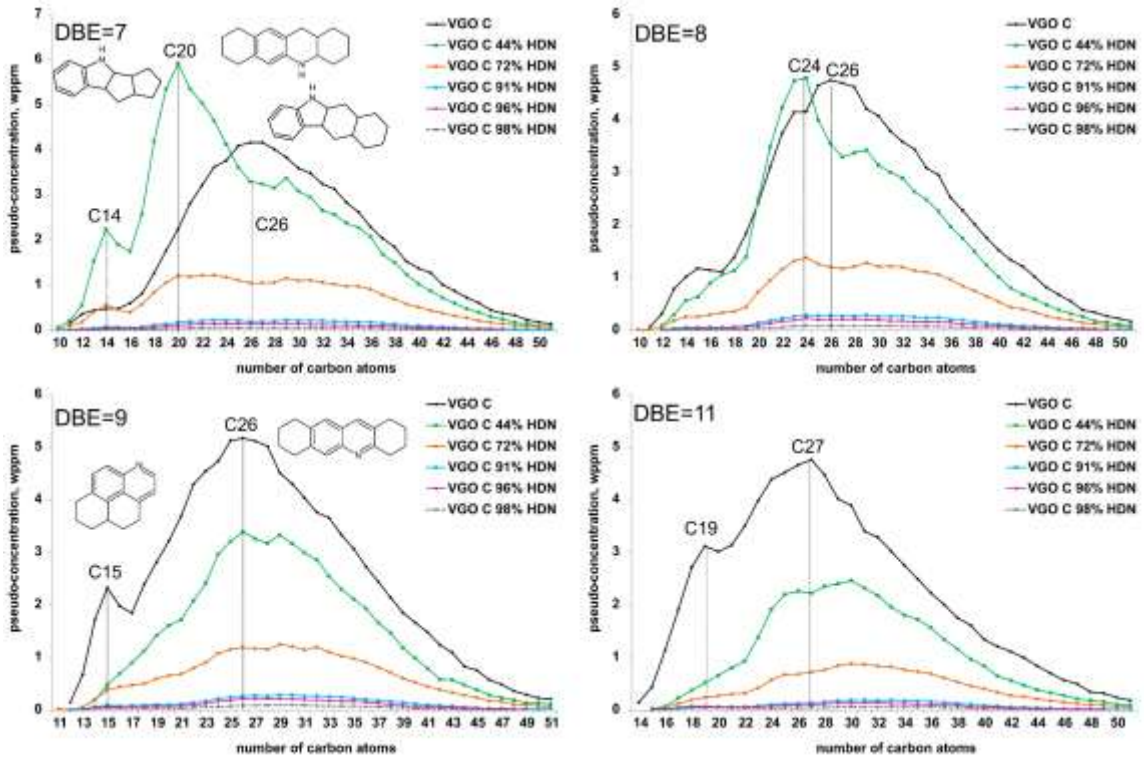

Fig. 9. The carbon number distributions of the quinolines (DBE=7-9) and acridines (DBE=11) in VGO C.

Returning to the carbon number distribution of neutral N-species, we noted that the initial increase in the pseudo-concentration of the DBE=10 compounds must be associated with hydrogenation of the abundant DBE=12 species (likewise, the hydrogenation of DBE=16 compounds shifts them to the DBE=14 family). At higher conversion, two peaks were observed in the carbon number distributions, at 16 and 23 carbon atoms. Species with 16 carbon atoms could be bare carbazole structures with one hydrogenated ring. However, these species were also present in the effluents of VGO A and B and did not have particularly low reactivity. We, therefore, evoke the hypothesis that the two peaks could be derivatives of refractory species described in the work of Wiwel et al. [25]., i.e. carbazole species with an additional hepta-cycle (4,8,9,10-tetrahydrocyclohepta-[def]carbazole). The bare structure has 15 carbon atoms, an analogous structure with two additional naphthenic cycles of 23 carbon atoms.

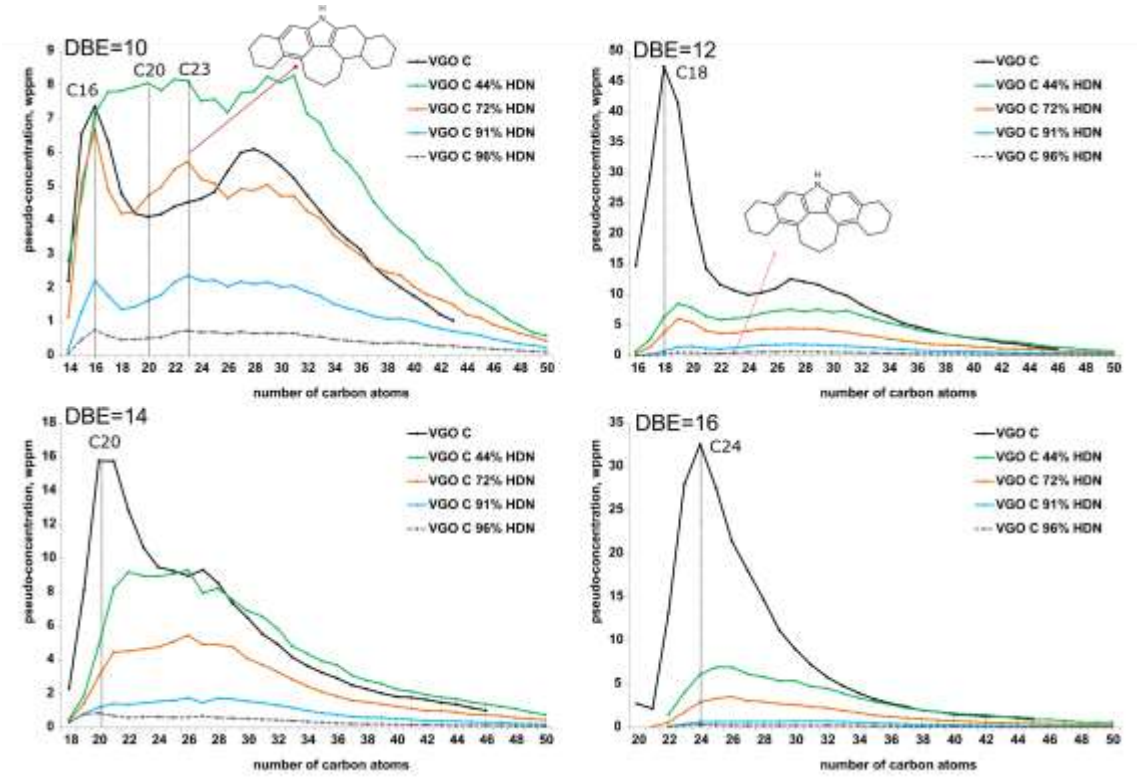

Fig. 10. The carbon number distributions of the carbazoles (DBE=10), benzocarbazoles (DBE=12 and 14) and dibenzocarbazoles (DBE=16) in VGO C.

441 *4.2.4. Changes in carbon number distributions for HVGO VGO D*

442 In the case of VGO D, there was a fast consumption of less alkylated basic species below 35
443 carbon atoms (Fig. 7), similar to VGO A. For neutral N-species, the maximum of distribution
444 remained at 32 carbon atoms (Fig. 8).

445 Fig. A.10 illustrates that the lighter species, which were quickly converted, mainly belonged to
446 DBE=9 and DBE=11 families. Conversion above 35 carbon atoms was initially very low. The
447 intermediate accumulation of the DBE=7 and 8 species around 34 carbon atoms can be attributed
448 to the hydrogenation of higher DBE compounds and to the transfer of neutral nitrogen species
449 (mainly benzocarbazoles, as already suggested for VGO C).

450 As for the neutral nitrogen species, we observed an accumulation of lighter neutral nitrogen
451 species with DBE=10, which can be linked to the hydrogenation of benzocarbazoles with higher
452 DBEs (Fig. A.11). Similarly to VGO C, we observed a peak at 15 carbon atoms and its slow
453 conversion with increasing severity of conditions, which can be related to the presence of the
454 refractory structures as 4,8,9,10-tetrahydrocyclohepta-[def]carbazole. But it is difficult to explain
455 the nature of the accumulation of nC15 compounds at the beginning of hydrotreatment.

456

457 **5. Discussion**

458 *5.1. Mechanisms of the VGO hydrodenitrogenation*

459 The previous two sections focused on the differences between the studied feeds in the HDN
460 process. Even though the analyzed feeds had different physicochemical properties and were of
461 different process origins, we can propose possible universal mechanisms for VGO HDN based on
462 the obtained DBE and carbon number distributions for each feed. Analyzing the behavior of the
463 basic nitrogen species within the degree of HDN conversion, one can conclude that the

transformation of quinolines with DBE=9 (or higher) into species with DBE=7 was common for all feeds. For the two SR feeds A and B, this DBE shift largely explains the evolution of the basic nitrogen species. Generally speaking, the hydrogenation of species with higher DBE (more than DBE=8) is the source of production for the basic species with lower DBE. The hydrogenation of a condensed aromatic ring generally leads to a -2 DBE shift; acridine species are an exception, since the central ring is preferentially hydrogenated, which leads only to a -1 DBE shift [14]; a -3 DBE shift occurs in the case of hydrogenation of an isolated aromatic ring. Fig. 11 shows the comparison of the weighted arithmetic mean DBE shift at the early hydrotreatment stage (the difference between VGO and the first hydrotreated effluent produced at low HDN conversion) and at the medium HDN stage (the difference between the first hydrotreated effluent obtained at low HDN conversion and the medium HDN conversion effluent) at a fixed number of carbon atoms. One can see that the reactions of hydrogenation of a condensed aromatic ring (-2 DBE shift) take place at low and medium alkylation degrees (at 25 and 35 carbon atoms) for SR VGOs. Regarding the medium HDN level, there was no dramatic change in DBE, or there even was a slight DBE increase at low alkylation degree, since the hydrogenation stage has already been passed in most species. We have also presented evidence that some of the basic species have been generated from the transformation of neutral ones. Especially in the case of heavy coker gas oil VGO C, this leads to very peculiar carbon number distributions in the effluents at intermediate HDN conversions.

Returning to the transformation of neutral nitrogen species, we also observed the trend of transformation of highly aromatic “source” species into species with lower DBE (and subsequent hydrogenation into the basic N-species). At the beginning of hydrotreatment, for all four feeds, the pseudo-concentration of species with DBE=10 was higher in the effluents than in the feeds as a result of rapid hydrogenation of benzocarbazoles and dibenzocarbazoles. In the case of HCGO,

we observed that the accumulation of species with DBE=10 in the effluents was higher than in other feeds. We relate it to the larger concentration of the carbazoles, dibenzocarbazoles, and the presence of the fourth peak of benzonaphtocarbazoles in the feed. All these families are sources for neutral N-species with DBE=10.

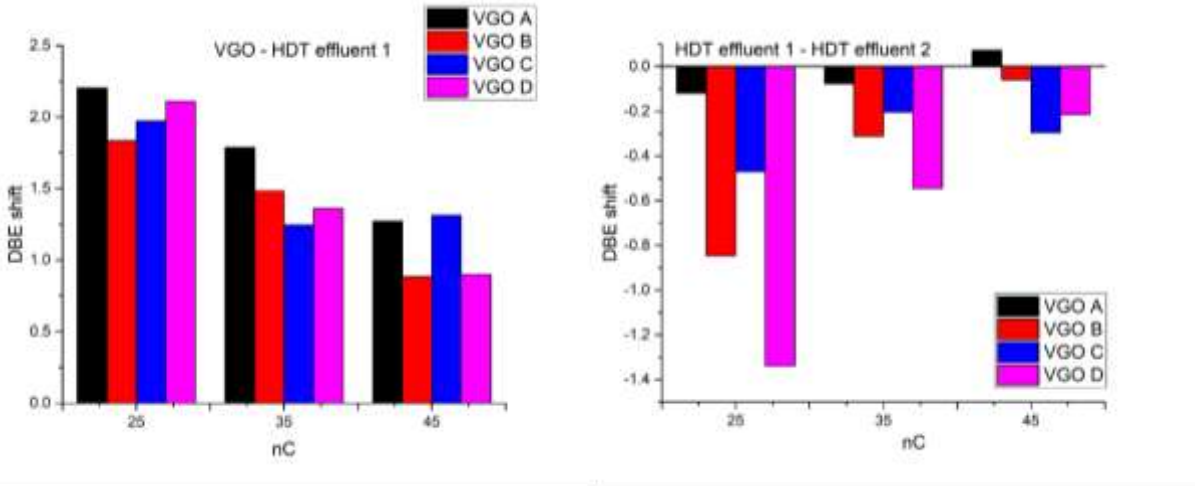

Fig. 11. The shift of the weighted arithmetic mean of DBE at the beginning of the hydrotreatment (VGO – HDT effluent 1) and the medium HDN conversion (HDT effluent 1 – HDT effluent 2).

An illustration of the mechanism of highly aromatic neutral species hydrogenation and generation of basic ones is illustrated using benzocarbazole as an example in Fig. 12. In the first step, hydrogenation of the side aromatic rings occurs, which leads to a shift to the left of the peaks in the DBE distribution within the HDN level. After hydrogenation of the aromatic ring next to the nitrogen-containing one, the character of the species becomes more basic, as the nitrogen atom's lone pair of electrons is no more involved in aromatic bonds, and therefore it will be ionized in positive ESI mode, and in the case of the illustrated example, we expect to see these species in the distributions of the basics with DBE=7. These steps of rings hydrogenation are essential before the subsequent cleavage of the C-N bond [39].

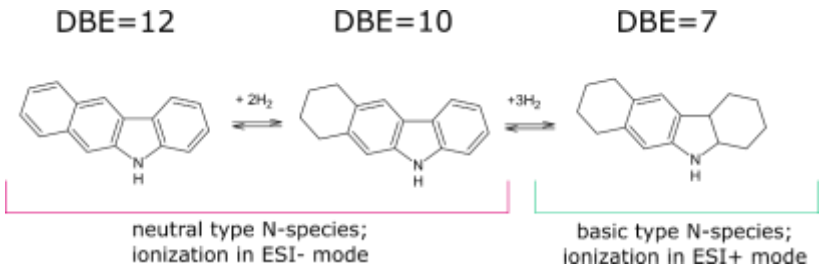

Fig. 12. The hypothetical mechanism for hydrogenation of highly aromatic neutral nitrogen species and their transformation into the basic N-species.

The results also showed differences between the studied feeds. One of the most remarkable results was the different reactivity of the neutral N-species. The light neutral species were more reactive than the heavy ones in VGO A and VGO D, whereas in VGO B and C the opposite was the case. The carbon number distributions for the basic and neutral fractions were mostly smooth and monomodal in SR VGOs (except for a small peak at C20 for neutral high DBE compounds), while feeds C and D exhibited bimodal distributions in the neutral fraction. Taken together, these results suggest a higher presence of the compounds proposed in the work of Wiwel et al. [25] in the feeds issued from residue conversion. It is crucial to note that VGO C, which showed different behavior in the detailed carbon number distributions of nitrogen species, shows global kinetics similar to the SR VGO s. It can thus be conceivably hypothesized that the carbon number of N-species does not affect the global reactivity of the VGO during hydrotreatment. The lowest reactivity of the VGO D may be due to the fact that the neutral species, as carbazoles, that have been generated from heavy residuals, are more refractory. Fig. 6 shows that the amount of these carbazoles in VGO D is higher compared to other feeds.

5.2. Comparison to HDN of gas oils

Obviously, in gas oils, the nitrogen species have lower DBE and nC values, which is determined by the final boiling point of the fraction, which is lower in gas oils. In a study of Nguyen et al.

[20], a mixture of straight-run gas oil and coker gas oil (the boiling point at 95 % of yield is 397 °C) was characterized by the most abundant species with DBE=7-9 (quinolines family) and carbon numbers C16-C24. In our case, the studied feeds also contain abundant species with the same DBE values but with higher numbers of carbon atoms. The question arises if the behavior of VGO during HDT will be similar to GO?

The following general trends were observed for the N1 basic nitrogen family during HDT. In the case of the light fraction, the DBE of the basic species shifted to the left from DBE=8 to DBE=6 due to hydrogenation reactions (-2 DBE due to ring hydrogenation). In the case of VGO, a -2 DBE shift of the DBE distribution maximum in the converted effluents was also observed (shift from DBE=9 to DBE=7). Fig. A.12 demonstrates the changes in weighted arithmetic mean of DBE with HDN in VGOs and a lighter fraction (GO) studied in the related work. Similar to the case of gas oils, a high concentration of the low aromatic species as THQ Anilines Pyridines (DBE = 4-6) was observed in the effluents at low and medium conversion HDN rates compared to the initial feed.

In contrast to basic compounds, neutral nitrogen compounds reacted differently in gas oils. In the case of gas oils, the concentration of all neutral compounds reduced sharply with an increasing degree of conversion compared to the VGO. At medium and high conversion rates, only small amounts of carbazoles (DBE=9) and tetrahydrobenzocarbazoles (DBE=10) remained in the HDT gas oil effluent, and their concentration remained approximately unchanged with the increasing conversion rate. In the case of VGO, there was an increase in the concentration of carbazoles (DBE=9-11) due to the conversion of species with higher DBE, such as benzocarbazoles, dibenzocarbazoles, and benzonaphtocarbazoles, which are present in very low concentrations in gas oils. We believe that the presence of these compounds led to a shift in the DBE distributions in the case of VGO.

5.3.Comparison to HDN of heavier fractions (residues)

In contrast to DBE changes in hydrotreated VGO effluents, in the study of Li et al.[40], a slight increase in DBE and alkylation degree of the basic nitrogen species within the hydrotreatment of atmospheric residue (AR) was observed. The authors suggest that it happens due to the removal of lighter molecules or (and) its condensation.

Neutral nitrogen components in the study of AR showed an increase in carbon number and a decrease in DBE through hydrotreatment. An interesting point here is that similar to the case of gas oils and VGOs (SR VGOs and HVGO), the DBE=10 was the most abundant in the most hydrotreated AR effluent. Similar to VGO, the initial AR and effluents at the beginning of the hydrotreatment had a high relative intensity of the dibenzocarbazoles (DBE=15), which probably were converted into benzocarbazoles with DBE=12/13 and carbazoles with DBE=10 via hydrogenation reactions.

6. Conclusions

Our study shows the differences in the N-species distributions at various HDN conversion degrees in feeds of different process origins obtained by the (ESI+/-)-FTICR-MS. DBE vs. a number of carbon atoms plots for two straight-run vacuum gas oils (SR VGO) characterized by differences in macroscopic properties, as the content of the total nitrogen, density, and sulfur, demonstrated similarities in the distribution of the most abundant peaks. The two feeds coming from residue conversion processes, however, exhibited a distinctly different distribution of nitrogen species, especially in the neutral fraction, which contained a high proportion of species with very high DBE values.

By comparing the DBE/carbon number patterns of effluents with the feed, the reactivity of species at specific DBE and carbon number values in the hydrotreating process can be figured out. For heavy coker gas oil, the effect of the transition of neutral nitrogen species to basic during hydrotreatment was clearly demonstrated. Also, for the other VGOs, neutral-to-basic N-species transition processes probably occur, but kinetic modelling needs to be done to confirm them.

When comparing the results with lighter and heavier fractions, it was noted that the refractory basic species are characterized by DBE=7 and DBE=8 (quinoline family). In the case of the refractory neutral species, in all feeds, there were carbazoles with DBE=10. However, in the case of VGO or heavier feeds compounds with DBE=12 and 13 remain also present in the effluents up to very high HDN levels, due to hydrogenation of neutral species with higher DBE values which are not present in gas oils.

In the discussion section, we have assumed that the carbon number of the species in the feed does not affect the HDN reactivity of the VGO, as we saw by an example of the VGO C. At the same time, we assumed that the low reactivity of the VGO D can be related to the more refractory character of carbazoles generated from heavy residues. Additional study of the isomeric structures of N-species probably will give an answer to the raised questions in this paper.

It is worth noting that a description of the reaction mechanisms and a selection of the versatile reactivity descriptors of VGO HDT remains very complex due to the fact that the residual basic and neutral N-containing structures are at the same time the result of the conversion of basic and(or) neutral N-families, as well as the initial unconverted structures (due to refractory character or due to competitive adsorption on the catalytic sites). At this level of data, we can observe only the main trends and the differences within HDN intensity depending on the processing origin of the VGOs. Understanding the structures of the selected species is still not possible at this level of

data, and it requires ion mobility and additional mass-spectrometry analyses, as the FTICR-MS analysis does not provide information on isomeric content. Chemometric tools, supplementary analytical data, and kinetic modelling will allow further interpretation of the data and a determination of a key refractory species in VGO hydrotreatment.

Appendices

Simplified scheme of the pilot unit **(Fig. A.1)**, comparison of the basic N1 families intensities in the samples prepared with 0.5 mg/mL and 1 mg/mL of VGO **(Fig. A.2)**, operating conditions and physicochemical properties of the HDT effluents **(Table A.1)**, description of the used analyses **(Table A.2)**, simulated distillation curves of vacuum gas oils **(Fig. A.3)**, explanation of the planar limit approach using the example of quinoline **(Fig. A.4)**, the simple hypothetical structures of the most abundant species in VGOs A-D **(Fig. A.5)**, the carbon number distributions of the quinolines (DBE=7-9) and acridines (DBE=11) in VGO A **(Fig. A.6)**, the carbon number distributions of the carbazoles (DBE=10), benzocarbazoles (DBE=12 and 14) and dibenzocarbazoles (DBE=16) in VGO A **(Fig. A.7)**, the carbon number distributions of the quinolines (DBE=7-9) and acridines (DBE=11) in VGO B **(Fig. A.8)**, the carbon number distributions of the carbazoles (DBE=10), benzocarbazoles (DBE=12 and 14) and dibenzocarbazoles (DBE=16) in VGO B **(Fig. A.9)**, the carbon number distributions of the quinolines (DBE=7-9) and acridines (DBE=11) in VGO D **(Fig. A.10)**, the carbon number distributions of the carbazoles (DBE=10), benzocarbazoles (DBE=12 and 14) and dibenzocarbazoles (DBE=16) in VGO D **(Fig. A.11)**, the weighted arithmetic mean of DBE as a function of HDN in VGOs and gas oil **(Fig. A.12)**.

Acknowledgments

This work was financially supported by IFP Energies Nouvelles and TotalEnergies, France.

References

[1] Girgis MJ, Gates BC. Reactivities, Reaction Networks, and Kinetics in High-pressure Catalytic Hydroprocessing. Ind. Eng. Chem. Res. 1991;30(9):2021–58. https://doi.org/10.1021/ie00057a001.

[2] Satterfield CN, Modell M, Wilkens JA. Simultaneous Catalytic Hydrodenitrogenation of Pyridine and Hydrodesulfurization of Thiophene. Ind. Eng. Chem. Process Des. Dev. 1980;19(1):154–60. https://doi.org/10.1021/i260073a027.

[3] Sumbogo Murti SD, Yang H, Choi K-H, Korai Y, Mochida I. Influences of Nitrogen Species on the Hydrodesulfurization Reactivity of a Gas Oil Over Sulfide Catalysts of Variable Activity. Applied Catalysis A: General 2003;252(2):331–46. https://doi.org/10.1016/S0926-860X(03)00468-X.

[4] Zeuthen P, Schmidt M, Rasmussen HW, Moyse BM. The benefits of cat feed hydrotreating and the impact of feed nitrogen on catalyst stability. NPRA Annual Meeting Technical Papers 2010;2:818–33.

[5] Stratiev D, Shishkova I, Ivanov M, Dinkov R, Georgiev B, Argirov G et al. Catalytic Cracking of Diverse Vacuum Residue Hydrocracking Gas Oils. Chem Eng & Technol 2021;44(6):997–1008. https://doi.org/10.1002/ceat.202000577.

[6] Vistisen PØ, Zeuthen P. Reactions of Organic Sulfur and Nitrogen Compounds in the FCC Pretreater and the FCC Unit. Ind. Eng. Chem. Res. 2008;47(21):8471–7. https://doi.org/10.1021/ie8006616.

[7] McIlvried HG. Kinetics of the Hydrodenitrification of Pyridine. Ind. Eng. Chem. Process Des. Dev. 1971;10:125–30. https://doi.org/10.1021/i260037a023.

[8] Raghuveer CS, Thybaut JW, Bruycker R de, Metaxas K, Bera T, Marin GB. Pyridine Hydrodenitrogenation Over Industrial NiMo/γ-Al2O3 Catalyst: Application of Gas Phase Kinetic Models to Liquid Phase Reactions. Fuel 2014;125:206–18. https://doi.org/10.1016/j.fuel.2014.02.017.

[9] Pille R, Froment G. Kinetic Study of the Hydrodenitrogenation of Pyridine and Piperidine on a NiMo Catalyst. Studies in Surface Science and Catalysis 1997;106:403–13. https://doi.org/10.1016/S0167-2991(97)80038-9.

[10] Nguyen M-T, Tayakout-Fayolle M, Pirngruber GD, Chainet F, Geantet C. Kinetic Modeling of Quinoline Hydrodenitrogenation over a NiMo(P)/Al2O3 Catalyst in a Batch Reactor. Ind. Eng. Chem. Res. 2015;54(38):9278–88. https://doi.org/10.1021/acs.iecr.5b02175.

[11] Satterfield CN, Cocchetto JF. Reaction Network and Kinetics of the Vapor-Phase Catalytic Hydrodenitrogenation of Quinoline. Ind. Eng. Chem. Process Des. Dev. 1981;20(1):53–62. https://doi.org/10.1021/i200012a008.

[12] Yang SH, Satterfield CN. Catalytic Hydrodenitragenation of Quinoline in a Trickle-Bed Reactor. Effect of Hydrogen Sulfide. Ind. Eng. Chem. Process Des. Dev. 1984;23(1):20–5. https://doi.org/10.1021/i200024a003.

[13] Prins R, Jian M, Flechsenhar M. Mechanism and Kinetics of Hydrodenitrogenation. Polyhedron 1997;16(18):3235–46. https://doi.org/10.1016/S0277-5387(97)00111-3.

[14] Rabarihoela-Rakotovao V, Diehl F, Brunet S. Deep HDS of Diesel Fuel: Inhibiting Effect of Nitrogen Compounds on the Transformation of the Refractory 4,6-Dimethyldibenzothiophene Over a NiMoP/Al2O3 Catalyst. Catal Lett 2009;129(1-2):50–60. https://doi.org/10.1007/s10562-008-9777-x.

[15] Bunch A, Zhang L, Karakas G, Ozkan US. Reaction Network of Indole Hydrodenitrogenation over NiMoS/γ-Al2O3 Catalysts. Applied Catalysis A: General 2000;190(1-2):51–60. https://doi.org/10.1016/S0926-860X(99)00270-7.
[16] Kim SC, Massoth FE. Kinetics of the Hydrodenitrogenation of Indole. Ind. Eng. Chem. Res. 2000;39(6):1705–12. https://doi.org/10.1021/ie9906518.
[17] Nguyen M-T, Pirngruber GD, Chainet F, Tayakout-Fayolle M, Geantet C. Indole Hydrodenitrogenation over Alumina and Silica–Alumina-Supported Sulfide Catalysts—Comparison with Quinoline. Ind. Eng. Chem. Res. 2017;56(39):11088–99. https://doi.org/10.1021/acs.iecr.7b02993.
[18] Boduszynski MM. Composition of Heavy Petroleums. 2. Molecular Characterization. Energy Fuels 1988;2(5):597–613. https://doi.org/10.1021/ef00011a001.
[19] Shin S, Sakanishi K, Mochida I, Grudoski DA, Shinn JH. Identification and Reactivity of Nitrogen Molecular Species in Gas Oils. Energy Fuels 2000;14(3):539–44. https://doi.org/10.1021/ef990136m.
[20] Nguyen M-T, Pirngruber GD, Chainet F, Albrieux F, Tayakout-Fayolle M, Geantet C. Molecular-Level Insights into Coker/Straight-Run Gas Oil Hydrodenitrogenation by Fourier Transform Ion Cyclotron Resonance Mass Spectrometry. Energy Fuels 2019;33(4):3034–46. https://doi.org/10.1021/acs.energyfuels.8b04432.
[21] Le Maître J, Hubert-Roux M, Paupy B, Marceau S, Rüger CP, Afonso C et al. Structural Analysis of Heavy Oil Fractions After Hydrodenitrogenation by High-Resolution Tandem Mass Spectrometry and Ion Mobility Spectrometry. Faraday Discuss 2019;218:417–30. https://doi.org/10.1039/C8FD00239H.
[22] Le Maître J, Paupy B, Hubert-Roux M, Marceau S, Rüger C, Afonso C et al. Structural Analysis of Neutral Nitrogen Compounds Refractory to the Hydrodenitrogenation Process of Heavy Oil Fractions by High-Resolution Tandem Mass Spectrometry and Ion Mobility–Mass Spectrometry. Energy Fuels 2020;34(8):9328–38. https://doi.org/10.1021/acs.energyfuels.0c01160.
[23] Wen S-C, Zhou Y-S, Wei Q. Hydrogenation Performance of Nitrogen Containing Compounds Present in Coker Gas Oil. Acta Petrolei Sinica (Petroleum Processing Section) 2008, 2008:496–502.
[24] Guillemant J, Berlioz-Barbier A, Oliveira LP de, Albrieux F, Lacoue-Nègre M, Duponchel L et al. Exploration of the Reactivity of Heteroatomic Compounds Contained in Vacuum Gas Oils during Hydrotreatment Using Fourier Transform Ion Cyclotron Resonance Mass Spectrometry. Energy Fuels 2020;34(9):10752–61. https://doi.org/10.1021/acs.energyfuels.0c01760.
[25] Wiwel P, Hinnemann B, Hidalgo-Vivas A, Zeuthen P, Petersen BO, Duus JØ. Characterization and Identification of the most Refractory Nitrogen Compounds in Hydroprocessed Vacuum Gas Oil. Ind. Eng. Chem. Res. 2010;49(7):3184–93. https://doi.org/10.1021/ie901473x.
[26] Celis-Cornejo CM, Pérez-Martínez DJ, Orrego-Ruiz JA, Baldovino-Medrano VG. Identification of Refractory Weakly Basic Nitrogen Compounds in a Deeply Hydrotreated Vacuum Gas Oil and Assessment of the Effect of Some Representative Species over the Performance of a Ni–MoS 2 /Y-Zeolite–Alumina Catalyst in Phenanthrene Hydrocracking. Energy Fuels 2018;32(8):8715–26. https://doi.org/10.1021/acs.energyfuels.8b02045.
[27] Merdrignac I. Composition des Structures Azotées dans les Pétroles. Implication pour leur Réactivité au cours des Procédés d'Hydrodésazotation. Université Louis Pasteur; 1997.

[28] Manek E, Haydary J. Hydrocracking of Vacuum Residue with Solid and Dispersed Phase Catalyst: Modeling of Sediment Formation and Hydrodesulfurization. Fuel Processing Technology 2017;159:320–7. https://doi.org/10.1016/j.fuproc.2017.02.003.
[29] Sahu R, Song BJ, Im JS, Jeon Y-P, Lee CW. A Review of Recent Advances in Catalytic Hydrocracking of Heavy Residues. Journal of Industrial and Engineering Chemistry 2015;27:12–24. https://doi.org/10.1016/j.jiec.2015.01.011.
[30] Meyers RA. Handbook of petroleum refining processes. 4th ed. New York NY: McGraw-Hill Education; 2016.
[31] Purcell JM, Rodgers RP, Hendrickson CL, Marshall AG. Speciation of Nitrogen Containing Aromatics by Atmospheric Pressure Photoionization or Electrospray Ionization Fourier Transform Ion Cyclotron Resonance Mass Spectrometry. J Am Soc Mass Spectrom 2007;18(7):1265–73. https://doi.org/10.1016/j.jasms.2007.03.030.
[32] Charon-Revellin N, Dulot H, López-García C, Jose J. Kinetic Modeling of Vacuum Gas Oil Hydrotreatment using a Molecular Reconstruction Approach. Oil Gas Sci. Technol. – Rev. IFP Energies nouvelles 2011;66(3):479–90. https://doi.org/10.2516/ogst/2010005.
[33] Klein GC, Rodgers RP, Marshall AG. Identification of Hydrotreatment-Resistant Heteroatomic Species in a Crude Oil Distillation Cut by Electrospray Ionization FT-ICR Mass Spectrometry. Fuel 2006;85(14-15):2071–80. https://doi.org/10.1016/j.fuel.2006.04.004.
[34] Mullins OC, Sheu EY, Hammami A, Marshall AG (eds.). Asphaltenes, heavy oils, and petroleomics. New York: Springer; 2007.
[35] Guillemant J, Albrieux F, Oliveira LP de, Lacoue-Nègre M, Duponchel L, Joly J-F. Insights from Nitrogen Compounds in Gas Oils Highlighted by High-Resolution Fourier Transform Mass Spectrometry. Anal Chem 2019;91(20):12644–52. https://doi.org/10.1021/acs.analchem.9b01702.
[36] Guillemant J, Albrieux F, Lacoue-Nègre M, Pereira de Oliveira L, Joly J-F, Duponchel L. Chemometric Exploration of APPI(+)-FT-ICR MS Data Sets for a Comprehensive Study of Aromatic Sulfur Compounds in Gas Oils. Anal Chem 2019;91(18):11785–93. https://doi.org/10.1021/acs.analchem.9b02409.
[37] Cho Y, Kim YH, Kim S. Planar Limit-Assisted Structural Interpretation of Saturates/Aromatics/Resins/Asphaltenes Fractionated Crude Oil Compounds Observed by Fourier Transform Ion Cyclotron Resonance Mass Spectrometry. Anal Chem 2011;83(15):6068–73. https://doi.org/10.1021/ac2011685.
[38] Nagai M, Masunaga T, Hanaoka N. Hydrodenitrogenation of Carbazole on a Mo/Al2O3 Catalyst. Effects of Sulfiding and Sulfur Compounds. Energy Fuels 1988;2(5):645–51. https://doi.org/10.1021/ef00011a007.
[39] Tominaga H, Nagai M. Reaction mechanism for hydrodenitrogenation of carbazole on molybdenum nitride based on DFT study. Applied Catalysis A: General 2010;389(1-2):195–204. https://doi.org/10.1016/j.apcata.2010.09.020.
[40] Li Y-E, Guan Y-M, Liu M, Yuan S-H, Zhang C, Song Y-Y. Transformation of Basic and Non-basic Nitrogen Compounds during Heavy Oil Hydrotreating on Two Typical Catalyst Gradations. Energy Fuels 2021;35(3):2826–37. https://doi.org/10.1021/acs.energyfuels.0c03028.